APL Electronic Devices

RESEARCH ARTICLE | APRIL 22 2025

Self-aligned laser opening and stencil metallization for silver-free contacts in silicon solar cells

Yuelin Xiong ; Ruidong Zhou; Anastasia Soeriyadi; Zongtao Liu; Soumyajit Maitra; Yifu Shi ; Jingyan Chen; John O'Sullivan; Matthew Wright ; Pietro Altermatt ; Ruy Sebastian Bonilla

APL Electronic Devices 1, 026109 (2025)
https://doi.org/10.1063/5.0250845

AIP Publishing

Self-aligned laser opening and stencil metallization for silver-free contacts in silicon solar cells

Cite as: APL Electron. Devices 1, 026109 (2025); doi: 10.1063/5.0250845
Submitted: 27 November 2024 • Accepted: 30 March 2025 •
Published Online: 22 April 2025

Yuelin Xiong,[1] Ruidong Zhou,[1] Anastasia Soeriyadi,[1] Zongtao Liu,[1,2,3] Soumyajit Maitra,[1] Yifu Shi,[1] Jingyan Chen,[1] John O'Sullivan,[1] Matthew Wright,[1] Pietro Altermatt,[2] and Ruy Sebastian Bonilla[1,a)]

AFFILIATIONS

[1] Department of Materials, University of Oxford, Oxford OX1 3PH, United Kingdom
[2] Trina Solar, State Key Laboratory for Photovoltaic Science and Technology (SKL PVST), Xinbei District, Changzhou, Jiangsu Province 213031, China
[3] Institute for Solar Energy Systems, School of Physics, Sun Yat-sen University, Guangzhou 510006, China

[a)] **Author to whom correspondence should be addressed:** sebastian.bonilla@materials.ox.ac.uk

ABSTRACT

Overreliance on silver in solar cell manufacturing places an immense challenge on sustainability. Terawatt-scale solar energy generation is required within the next few decades, and current attempts to replace silver screen printing are inferior compared to conventional techniques. This work reports on a novel metallization methodology using a UV picosecond laser to ablate textured surface dielectric layers in a pattern defined by an *in situ* stencil shadow mask. Since the stencil mask does not need to be removed, a metal contact can be directly deposited employing printing or vapor deposition in one integrated process. Here, we demonstrate 26 μm wide metal fingers via thermally evaporated aluminum directly deposited onto laser-patterned point contacts of 16.9 × 19.1 μm^2 size. Optical and electron microscopy analysis shows that the UV picosecond laser ablation damage is limited, and sufficient alignment is achieved. A line resistivity of 15.74 ± 2.35 Ω/cm and a contact resistivity of <10 mΩ·cm^2 show the current-carrying capabilities of the contacts. Complete solar cell devices were produced using our new stencil self-aligned contacts, and electrical measurements show a pseudo-efficiency of 18.8%. This novel approach could potentially lead to a replacement of non-sustainable silver as front and back contacts for bifacial solar cells.

I. INTRODUCTION

Climate change mitigation requires the deployment of terawatt-scale solar energy. Since the current solar cell architectures rely heavily on silver for front and rear contacts, this will lead to a vast increase in the demand for this metal. The burden on silver supply and solar cell costs will become unsustainable if the screen-printing process with silver pastes is to be continued.[1–3] New methodologies to metallize solar cells without the use of silver are hence urgently required. One such possibility is aluminum. However, screen printing with aluminum pastes cannot achieve the industrial requirements of 20–30 μm finger width[4] since typical aluminum pastes comprise large spherical Al and Al–Si alloy powders with a 6–8 μm diameter. In industry, such pastes could only produce wide metal fingers of 60–90 μm width.[5] Because of the aluminum oxide layer forming at powder surfaces, weak bonding and linkage between powder particles cannot keep the particles in a stable position, resulting in a collapse during the firing process and wider contacts, which, in turn, affect the solar cell performance.[6,7] Hybrid metallization approaches that combine aluminum and silver paste have also been proposed to allow fire-through processes. Yet, these cause metallic spiking during the firing and cooling process, which leads to junction current leaking and adversely impacts reliability.[8,9] Overall, while aluminum-based metallization benefits from a scalable supply chain, it requires alternative processing routes that meet the stringent constraints of terawatt-scale manufacturing.

Studies have demonstrated that laser processing enables low-damage contact openings in AlO_x/SiN_y layers. In particular, optimized UV picosecond laser parameters have been successfully applied for the patterned, near damage-free ablation of the rear-side AlO_x/SiN_y stack in the passivated emitter and rear cell (PERC) solar cells.[10,11] A critical aspect of metallization in non-screen-printing techniques is alignment, which ensures precise matching of metal fingers with laser-ablated openings in the passivation layer, enabling accurate and efficient alternative metal deposition. Qian *et al.* reported challenges in aligning local printing to these laser openings. In their work on bifacial PERC, aluminum fingers were required to extend 78 μm beyond the 42 μm-wide ablation lines to accommodate alignment tolerances.[12]

In this work, we introduce a novel self-aligned metallization process. We fabricate and place stainless steel stencil masks on the top surface of a silicon substrate, followed by laser ablation and thermal evaporation of aluminum through the shadow mask. Optical microscopy and scanning electron microscopy (SEM) were used to investigate laser ablation damage and the level of alignment achieved by this process. Device analysis methods were used to characterize electrical performances and contact quality. This approach can be adapted to other solar cell metallization techniques, including emerging metal pastes that do not require frit-etching, as well as physical vapor deposition methods that demand high-precision self-alignment.

II. SAMPLE PREPARATION AND METHODOLOGY

A. Process scheme

Figure 1 schematically illustrates the processing steps for the front metallization of TOPCon solar cells. Standard 150 μm-thick Tunnel Oxide Passivated Contact (TOPCon) solar cell precursors were sourced from an industrial manufacturer. These precursors featured an n-type silicon base with a resistivity of 0.3–2.1 Ω·cm, a textured front surface coated with an AlO_x/SiN_y passivation stack, and a rear-side tunnel oxide layer with an n^{++}poly-Si contact, as shown in Fig. 1(a).

In this method, a stencil mask was placed on the substrate and mechanically secured using magnets. As shown in Fig. 1(b), a UV picosecond laser was then raster-scanned perpendicular to the length of the fingers to create point contacts. The contact area between the silicon and metal was controlled by adjusting the number of raster lines. Figure 1(c) illustrates the thermal evaporation of aluminum, performed while the stencil mask remained in place to ensure precise alignment between the openings and metal deposition. Figure 1(d) shows the final front metallization structure.

B. Stencil mask fabrication

The stencil masks for these substrates were fabricated using 170 μm thick stainless-steel sheets via an LX-A1 1064 nm nanosecond pulsed 20-W infrared (IR) laser machine. Due to the high absorption of IR laser wavelengths by metals, efficient energy conversion into heat enables precise melting and vaporization of the metal sheet during cutting.[13] Stainless steel was chosen over commonly used brass masks for its ferromagnetic properties, which allow for secure magnetic affixing. The selected mask thickness was optimized to minimize bending during laser processing while ensuring compatibility with the laser opening process. The dimensions and edge smoothness of the mask openings were controlled by adjusting key laser parameters, including laser current, raster scan

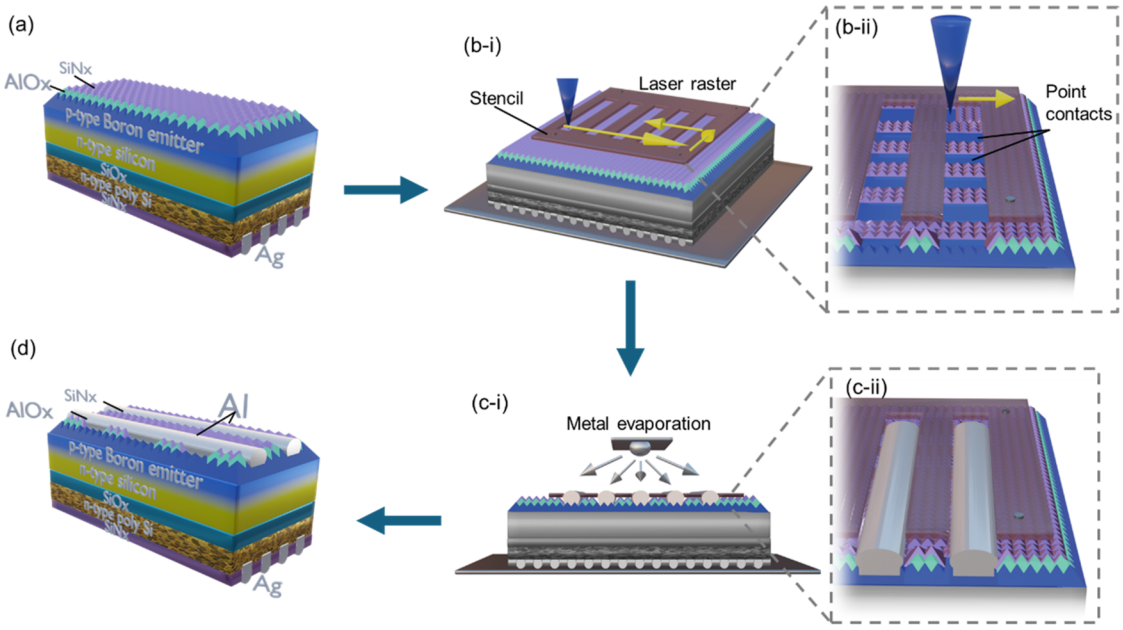

FIG. 1. Schematic diagram of the fabrication process for the metallization method presented in this work: (a) initial TOPCon precursor with a textured front surface, a front AlO_x/SiN_y passivation stack, and a rear-side tunnel oxide layer with an n^{++}poly-Si contact, (b) laser ablation through a stencil to create periodic point contacts, (c) thermal evaporation of aluminum over the laser-defined openings, and (d) final front metallization structure.

speed, pulse repetition rate, and the number of loops. The optimized laser parameters were determined through a factorial experiment design, systematically varying each parameter and measuring the resulting opening width using an optical microscope (Olympus BX51M) to assess their combined effects.

Neodymium N35 magnets were used to attach the stencil mask and sample substrate to achieve stable attachment during processing steps, including high-temperature annealing. This eliminates the risk of tape decomposing and ensures more reliable results.

C. Laser contact fabrication

An Inggu GXP 355-5 355 nm UV picosecond pulsed laser was used to ablate the front surface of the TOPCon solar cells, creating laser contact openings in the AlO_x/SiN_y stack while minimizing damage to the underlying silicon.[14,15] The optimization process of laser contact openings is detailed in Sec. III B.

The laser opening shape and width were characterized using optical microscopy. Scanning electron microscopy (SEM, Zeiss EVO) was employed to examine the fabricated front contact. Photoluminescence (PL) imaging was used to visualize carrier density under stable illumination, providing insight into spatial recombination, which is critical for minimizing recombination losses at the metallization.[16,17] The PL image was processed with a point spread function and a flat-field correction with LumiTools 2.0.

Aluminum deposition was performed via thermal evaporation (Vac Techniche DTE-170) at a working distance of 10 cm. The metal source was positioned directly above the sample, with a deposition rate of 2 nm/s, achieving a final metal thickness of 800 nm. For industrial applications, in-line high-rate evaporation provides a promising approach to achieving metal thicknesses that meet industry standards.[18]

D. Electrical characterization

A series of electrical characterization methods were conducted on the metal contacts, including line and contact resistivity measurements, to evaluate the contact properties. Device performance was investigated via dark and light current density–voltage (J–V) characteristics and Suns-V_{oc} analysis. These measurements provided insights into the performance of the metallized solar cells.

1. Line resistance

Line resistance was measured using a Keithley 2401 source measure unit (SMU) to assess the current extraction along the metal contacts. Figure 2 illustrates the experimental setup for these measurements. Two tungsten probes were positioned at different positions along the metal finger to measure the voltage drop, with probe spacings of 1, 2, 3, 4, and 5 mm. The measurement setup was visualized using a probe station equipped with an optical microscope and an integrated ruler to ensure precise alignment of the probes. This process was repeated across different evaporation batches and metal fingers to obtain an average value. It was assumed that the underlying silicon substrate has a significantly higher resistance than the metal, ensuring that current flows exclusively through the metal fingers. The finger width was measured using optical microscopy, while the height was determined from crystal monitor readings in the thermal evaporation system.

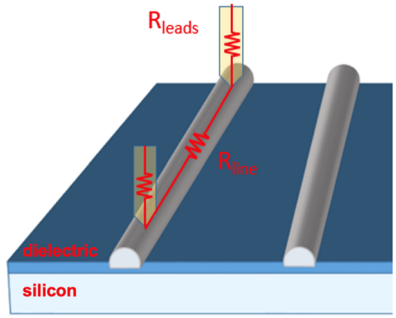

FIG. 2. Schematic diagram of the experimental setup for line resistance measurements.

2. Contact resistivity

Figure 3(a) illustrates the method employed in this work to determine the contact resistivity of the optimized laser-ablated contact structure. Due to the design of the sample structure used here, the effective metal contact length cannot be directly measured as it differs from the total length of the metal finger typically assumed in standard transmission line methods (TLMs).[19] To address this, the standard TLM equation was rearranged to remove the metal contact length as an input parameter. The resulting test structure is thus a modified version of the actual contact design, consisting of two metal lines separated by a fixed distance, while the Al/Si contact area is systematically varied. The contact area A_c is defined as the region where aluminum and silicon are in direct contact through the laser-ablated openings and is determined using optical microscopy. The contact area was adjusted by varying the number of laser-ablated openings beneath each metal line; specifically, 5, 10, 20, or 30 openings were used to control the metal contact area. Consequently, four samples were required to determine the contact resistivity. The total resistance can be described as

$$R_{total} = R_{metal} + R_{semi} + 2R_c,$$

which, under the assumption that the metal resistance is negligible, simplifies to:

$$R_{total} = R_{semi} + 2\frac{\rho_c}{A_c}.$$

By plotting R_{total} against $\frac{1}{A_c}$, contact resistivity ρ_c can be extracted from the gradient of the linear fit.

However, accurately determining the true active contact area A_c is challenging due to current crowding, which results in a non-uniform current distribution across the point contacts. In this study, the measured contact area is assumed equal to A_c. Consequently, the extracted contact resistivity inherently includes the current crowding effects.

Since contact resistivity is an intrinsic property that depends only on the laser ablation parameters for a given sample system, its value remains consistent across different structures. As the previously described method is too complex for the initial stage of process optimization, the standard TLM approach was applied to a different sample structure for laser parameter optimization. Figure 3(b) shows the contact structure. TLM samples were prepared by cutting a standard solar cell structure into strips perpendicular to the

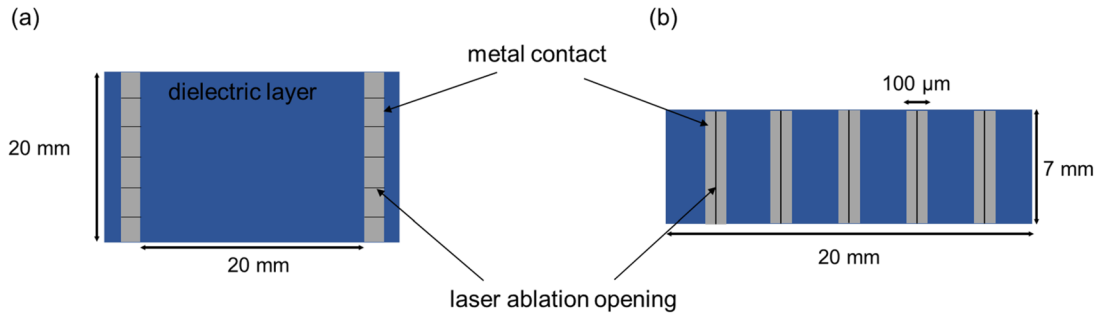

FIG. 3. Top view of (a) the method used to determine the contact resistivity of the optimized laser-ablated structure and (b) the standard TLM test structure for laser parameter optimization. Laser ablation lines (black) and metal fingers (gray) are shown schematically and not to scale.

metal fingers.[20,21] This configuration simplifies sample preparation for the initial stage of process optimization and minimizes current crowding in contact resistivity calculations, enabling a more reliable comparison of laser parameters to identify those that achieve the lowest contact resistance.

E. Device characterization

Electrical characterization of the finished cell structure was carried out to analyze the contact's performance at a device level. For comparison, two samples were analyzed. The first sample was a finished industrial reference TOPCon cell, which was laser-cut to 15 × 15 mm^2 using an LX-A1 1064 nm nanosecond pulsed 20-W infrared (IR) laser machine.[22] The industrial reference has the same front passivation stacks and texturing as the TOPCon precursor [Fig. 1(a)] but includes silver screen-printed front metallization, which was sourced from the same manufacturing line. The second was produced using the front metallization method proposed in this work, featuring 26 μm wide fingers made with the optimized laser ablation parameters. It was cut into a 12 × 12 mm^2 specimen using the same processing method as the reference.

Dark J–V curves were measured using a Keithley 2401 SMU in a four-wire configuration within a dark box and later fitted to a model for parameter extraction. A dark mask was used to limit the illuminated area to 10 × 10 mm^2 while also serving as the electrical connection to the front contact. For light J–V measurements, a LOT-QuantumDesign Europe LS0505 sun simulator was used under standard testing conditions, with an air mass 1.5G spectrum at an intensity of 100 mW/cm^2, calibrated using a standard silicon reference cell. Uniform illumination was provided over a 40 × 40 mm^2 area at 25 °C, regulated by a thermal control system. A Sinton Instruments Suns-V_{oc} system was used for Suns-V_{oc} measurements.

III. RESULTS AND DISCUSSIONS

A. Stencil mask dimensions

The optimized laser parameters for patterning the stainless-steel mask were used to produce a mask with a small opening size. Figures 4(a) and 4(b) illustrate the successful fabrication of a mask with an opening width of 20 μm, which is comparable to projected finger width dimensions achievable in the industry by 2030, as forecasted by ITRPV.[4]

B. Optimization of laser ablation parameters

Optimization of laser parameters for contact opening was carried out in three stages, with the parameter range refined at each step.[23] The optimization process involved varying the laser current and scanning speed. In the first stage, laser currents of 2–10 A and scanning speeds of 250–1000 mm/s were applied to laser ablation lines. The ablated areas were then visually examined using an optical microscope. Figure 5 presents an example of an optical microscope

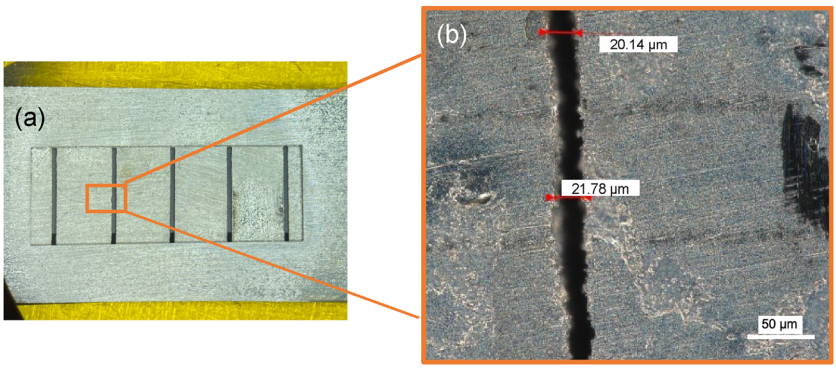

FIG. 4. (a) Image of the stencil mask and (b) optical micrograph of the stencil mask opening.

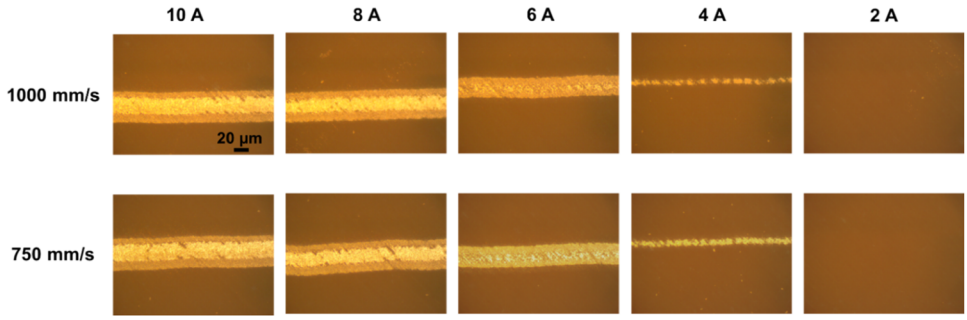

FIG. 5. An example of the optical microscope images of the laser current for a range of 2–10 A and laser scanning speeds of 750 and 1000 mm/s.

image of the patterned regions with laser current for a range of 2–10 A and laser scanning speeds of 750 and 1000 mm/s. Based on the morphology and width of the ablated lines, the laser conditions were further refined to a laser current range of 4–6 A and a scanning speed range of 700–900 mm/s.

In the second stage, PL imaging was used to identify parameters that cause severe laser damage and, consequently, degrade the overall solar cell performance. A 45 × 45 mm^2 TOPCon precursor with rear metallization was patterned on the front side with nine blocks of laser ablation parameters, each containing ten lines of 10 mm in length, spaced 1 mm apart. The ablation region of 10 × 10 mm^2 was large enough to be captured with high resolution by the CCD camera. The resulting PL image is shown in Fig. 6. Based on the previously narrowed range of laser current and scanning speeds, the PL image reveals that conditions with a laser current of 6 A lead to cell degradation. This allows a further refinement of processing parameters to the laser current range of 4–5 A and a scanning speed range of 700–900 mm/s.

It is also worth noting that the results demonstrate that edge damage caused by laser sample cleaving introduces significant recombination losses. In particular, the left and right edges in Fig. 6 exhibit more damage due to laser cleaving, whereas the bottom edge, which is the original sample edge, shows less severe edge recombination effects. This highlights a pre-existing loss mechanism that could influence solar cell properties.

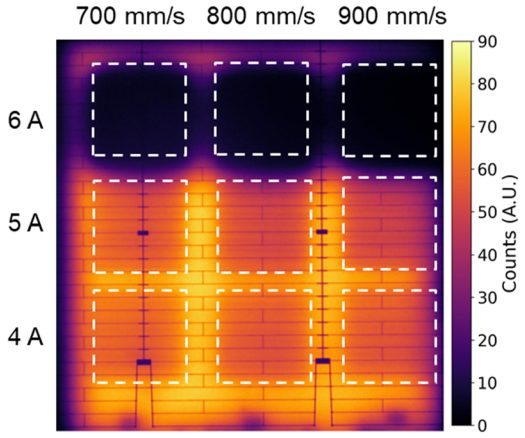

FIG. 6. Photoluminescence image of a 45 × 45 mm^2 sample processed under different laser conditions as part of the laser parameter optimization process, with currents ranging from 4 to 6 A and laser scanning speeds from 700 to 900 mm/s. White dashed squares indicate the laser ablation areas. Each square consists of ten laser lines, each 10 mm long and spaced 1 mm apart.

The final optimization step was carried out based on contact resistance with the experiment setup in Fig. 3(b). Table I presents the different laser ablation parameters, with increasing laser current from sample a to sample d, along with the corresponding contact resistance values. Excessive fluence can damage the silicon substrate, whereas insufficient fluence may fail to fully penetrate the dielectric layer, resulting in a non-ohmic contact. The laser parameters that yielded the lowest contact resistance, highlighted in gray, were selected for further experiments. We note here that the optimized laser parameters are dependent on the specific conditions of the laser and optical setup, but we provide them here for completeness.

C. Fabrication of laser point contacts

TOPCon precursor samples were processed using the optimized laser parameters with the mask *in situ* to selectively ablate the dielectric layers at periodic locations, enabling the formation of point contact openings along the metal fingers. Figure 1(b) illustrates the schematic of this structure, while Fig. 7 provides an optical microscopy image illustrating the size and pattern of the ablated areas, demonstrating the precise formation of laser-defined openings using metal masks. Following the optimization of the stencil mask manufacturing and laser ablation processes, the contact size was successfully reduced to 16.9 × 19.1 μm^2.

To examine the morphology of the metal contacts, samples with evaporated metal were prepared. Figure 1(c) illustrates the schematic of this structure, and Fig. 8 presents the top-view micrographs of the evaporated metal finger. The SEM image in Fig. 8(a) shows the

TABLE I. Summary of laser parameters and their corresponding contact resistance values for the fabricated samples a–d.

Laser parameters	Sample a	Sample b	Sample c	Sample d
Speed (mm/s)	900			
Current (A)	3.8	4	4.2	4.4
Contact resistance (Ω)	No ohmic contact	32.75	22.57	No ohmic contact

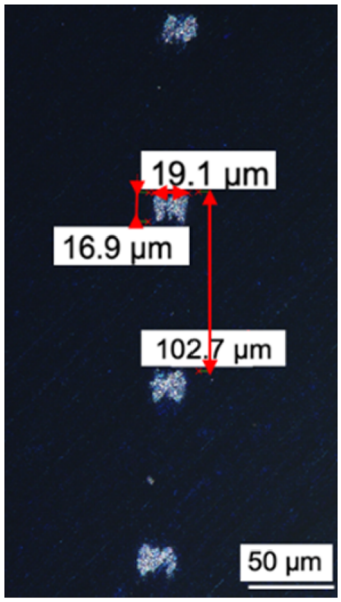

FIG. 7. Optical micrograph of the laser contact openings of 16.9 × 19.1 μm^2.

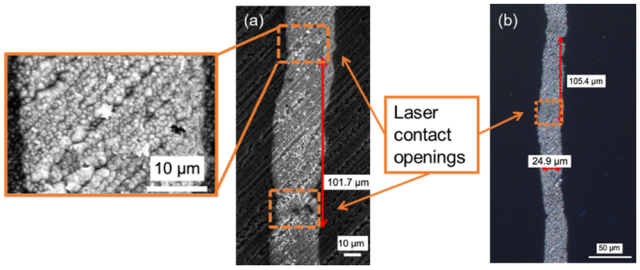

FIG. 8. (a) SEM images of the metal fingers showing the laser contact openings and (b) optical micrograph of the metal fingers.

laser contact openings, where a designed pitch length of 100 μm and a measured pitch length of 101.7 μm confirm the precise control of the laser patterning. The pitch length can be readily adjusted by modifying the laser ablation pattern to optimize efficiency, demonstrating the adaptability of this method. The laser ablation damage to the silicon surface appears minimal in this figure, with additional micrographs of the contacts provided in Fig. S2 for further analysis.

Figure 8(b) shows an example of an evaporated finger with a measured width of 24.9 μm, which meets industry standards. However, the metal finger width was slightly larger than the stencil mask opening, suggesting that metal evaporation extended beneath the stencil mask due to a small gap between the mask and substrate. To evaluate the uniformity of finger widths across multiple locations, we performed a width distribution analysis. The average finger width was found to be 26.3 μm with a standard deviation of 1.8 μm, demonstrating good uniformity and validating the precision of our stencil mask process (Fig. S3). These surface morphology analyses confirm that the *in situ* mask effectively localizes laser contact openings, enabling the formation of high-quality aluminum contacts with controlled pitch and consistent finger widths.

D. Electrical properties

Electrical measurements were conducted on the metalized samples using the methods detailed in Sec. II to demonstrate the effective metallization properties. The average line resistivity of the evaporated Al finger is 15.74 ± 2.35 Ω/cm for a finger height of 800 nm and a width of 26 μm. The line resistivity data of the thermally evaporated aluminum contacts have been included in the supplementary material (Fig. S1). This value is 17.5 times higher than the reported value for standard screen-printed Ag fingers, which was 0.9 Ω/cm for a typical cross-sectional area of 500 μm^2.[24] These results demonstrate the possibility for the evaporated contacts to be used for solar cells but also highlight the need to optimize the evaporation process further to create a solar cell metallization technique with improved performance. As a potential route to overcome the small-cross-section contacts, in-line high-rate evaporation could be used to increase the height and contact area, thereby achieving lower line resistivity.[18] Additionally, as silicon solar cells advance toward higher efficiencies, the precise alignment of locally highly doped emitters with metal fingers becomes increasingly important in metallization to minimize contact resistance.[25] The elevated temperatures at 850 K used in the in-line evaporation process could potentially facilitate the formation of a local aluminum back surface field (Al-BSF), which may enable the development of a self-aligned local selective emitter (Al-p^+).[26] However, these potential advantages require further investigation to confirm their practical effectiveness in industrial solar cell manufacturing.

Using the optimized parameters to ablate the dielectric layer of the test structure, the method described in Fig. 3(a) resulted in a contact resistivity of 1.39 mΩ cm^2 with an error margin of 10%, yielding values comparable to those of screen-printed contacts.[27] This indicates the potential of the contact formation technique via laser contact opening and metal evaporation, which was also demonstrated in previous work using a similar process.[28]

We then fabricated a sample solar cell using our metallization method and compared its performance to a reference TOPCon cell. Further analysis was carried out to characterize the device configuration under standard light operating conditions. Figure 9(a) shows the light J–V curve under 1-sun illumination and the pseudo-J–V curve obtained from Suns-V_{oc} measurements. Figure 9(b) shows the schematic diagram of the front structures of the samples. InGa paint was applied to a small point on the contact to establish a reliable connection between the sample and the measurement probe station, ensuring accurate measurement. The industrial reference cell was measured using a standard single-point probe on the busbar. Comparing the light J–V and the pseudo-J–V curves, it can be observed that the pseudo-J–V curve exhibits a sharper turn, whereas the light J–V curve is flatter. This indicates that series resistance contributions hamper operation under standard testing conditions. This is expected because of the high line resistivity obtained.

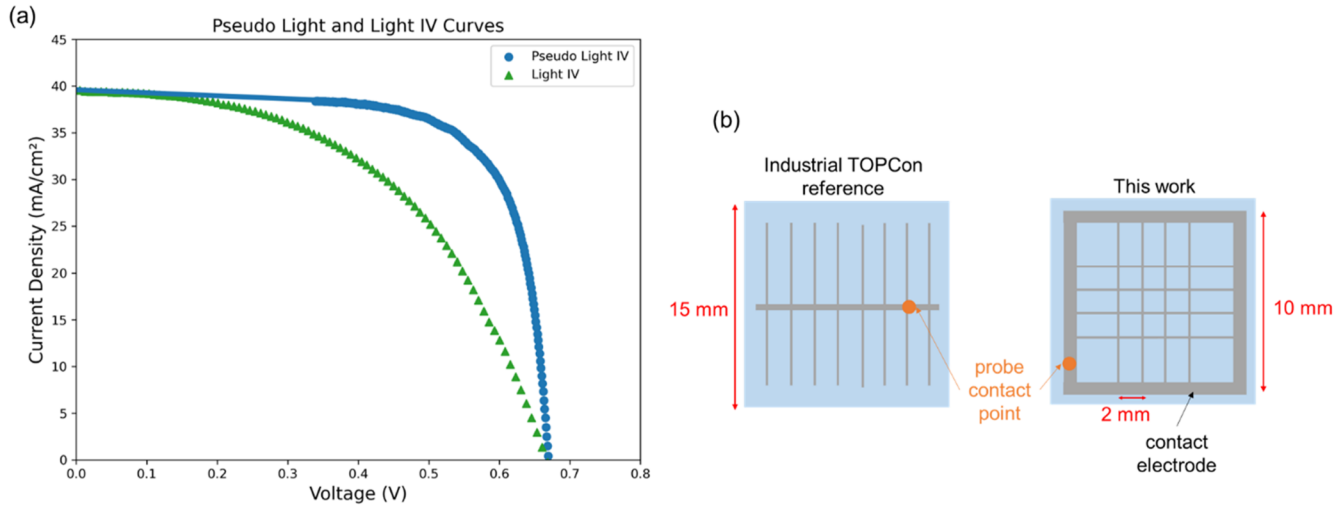

FIG. 9. (a): Light J–V under 1-sun simulation and pseudo-J–V curve based on Suns-V_{oc} of the laser-processed solar cell. (b) Schematic diagram of the front contact patterns used for the measurement.

Table II compares the performance of an optimized laser-processed cell from this study with a reference industrial cell. The maximum solar cell efficiency achieved for the laser-processed cell in this work is 13.2%, with all electrical parameters lower than those of the industrial reference. The open-circuit voltage (V_{oc}) of a solar cell depends on the recombination losses, which are primarily determined by material quality. In this study, the low V_{oc} values observed in both the laser-processed and reference cells indicate increased recombination losses. This trend is further supported by the iV_{oc} statistics presented in Fig. S5. A key contributing factor is edge recombination, likely introduced by the laser cleaving process.

The series resistance (R_s) for the laser-processed cell was extracted from the slope of the J–V curve near V_{oc} and was found to be higher than that of the reference cell. The higher value was expected as the metal height in this work has not yet been optimized to achieve industrial-level resistivity. A high R_s also reduces the fill factor (FF) in this study. Additionally, the short-circuit current density (J_{sc}) is lower than that of the reference cell despite a lower shading fraction. This suggests that high series resistance significantly affects current extraction. Several factors contribute to the high R_s observed in this study. First, the small height of the metal fingers results in higher line resistivity. Second, the absence of busbars, which are typically used in standard structures for effective current collection, limits the flow of current. The limited metal coverage for the test structure also contributes to the high R_s.

Suns-V_{oc} results in Table III, which shows an improvement in efficiency compared to the light J–V results due to the absence of series resistance in this technique. For Suns-V_{oc} measurements, the previously measured J_{sc} value of 39.6 mA/cm^2 was used. The improved pseudo-fill factor (pFF) and pseudo-efficiency (pη) compared to the J–V measurements in Table II suggest that series resistance is a primary limiting factor in solar cell performance, which may be exacerbated by the single-point electrical measurement. Alternatively, the lower FF could also result from additional recombination losses, likely introduced by the cleaving process.

Across all characterization techniques used in this study, the results consistently indicate high recombination losses and elevated R_s, both of which negatively impact device performance and contribute to efficiency losses compared to industrial TOPCon efficiencies (>23.4%).[22] These losses are largely influenced by sample processing and design factors. The laser cleaving process, in particular, introduces defects that increase recombination losses at the specimen edges. Figure 6 highlights significant edge damage from laser cleaving, which negatively impacts both the reference and the

TABLE II. Solar cell parameters extracted from 1-sun J–V measurement, for the laser-processed cell and the industrial TOPCon reference.

Sample	V_{oc} (mV)	J_{sc} (mA/cm^2)	FF (%)	Efficiency (%)	R_{series} (Ω cm^2)
This work	667	39.6	49.9	13.2	4.5
Reference	670	40.1	57.3	15.4	0.8

TABLE III. Solar cell parameters extracted from Suns-V_{oc} J–V measurement for the laser-processed cell and the industrial TOPCon reference.

	iV_{oc} (mV)	Ideality factor (n)	pFF (%)	pEfficiency (%)
This work	685	1.4	71.0	18.8
Reference	682	1.8	70.9	18.9

laser-processed cell. However, laser cleaving damage is not relevant in industrial settings and could potentially be minimized in research environments through fine optimization of the laser cleaving process. Despite the non-optimized cleaving process, pFF and pη remain relatively high, suggesting that the cell has strong performance potential if series resistance losses are mitigated. Griddler 2.5, a finite element method solver, was used to estimate the potential performance of our point-contact self-aligned method by analyzing the full metallization pattern and simulating the IV characteristics of the solar cell.[29] This simulation, presented in Fig. S4, shows promising cell performance with reduced line resistivity. Further optimization of the metallization design and processing steps is necessary to minimize series resistance and recombination losses, thereby enhancing the overall performance of the solar cell.

IV. CONCLUSIONS

We report an innovative and simple approach to self-aligning laser opening and stencil metallization using thermally evaporated Al as a substitute for Ag in solar cell fabrication. This quick and flexible process of fabricating Al contacts via perpendicular laser rastering provides a new economically viable and sustainable metallization technology that can be potentially implemented on industrial scales and is compatible with other metal deposition methods.

Point contacts with a width of 20 μm were achieved through precise laser parameter optimization. Surface morphology characterizations illustrate the precise control of laser contact and the achievement of thin metal contacts with metal evaporation. These findings show the feasibility of the developed methodology for solar cell metallization.

We then characterized the electrical and loss properties of the manufactured metal contacts. While the line resistivity is higher than the industry standard, this is due to the low metal height, which can be readily modified with other metal deposition techniques. The contact resistivity obtained in this work is comparable to industry standards. Finally, solar cell analysis showed the feasibility of developing functional cells with the proposed metallization method. However, performance fell short of industry standards due to sample design and preparation issues, which will be addressed in future work. This study offers a promising approach toward sustainable terawatt-scale photovoltaics, providing a novel solution for the industry's growing energy demands.

SUPPLEMENTARY MATERIAL

The supplementary material encompasses further details of the results in this work are provided, including the line resistivity data of the metal contact, SEM images of surface morphology, finger width distribution, Griddler simulation of the cell potential, and iV_{oc} results from Sinton Suns-V_{oc} measurements.

ACKNOWLEDGMENTS

All the authors are thankful to Radka Chakalova for assistance in clean-room processing. R.S.B. was supported by the Royal Academy of Engineering under the Research Fellowship scheme (Grant No. RF\201819\18\38). M.W. was supported by UK Research and Innovation (UKRI) under the UK government's Horizon Europe funding guarantee (Grant No. 101109417). A.S. was funded by the British Council under the PAK-UK ICRG 2020 project (No. 006327/D/ISB/008/2021). This work was supported by the UK Engineering and Physical Sciences Research Council (Grant No. EP/V038605/1), the Oxford University John Fell Fund, and the Leverhulme Trust Research Project Grant (RPG-2020-377). The authors acknowledge the use of characterization facilities within the David Cockayne Center for Electron Microscopy, Department of Materials, University of Oxford, alongside financial support provided by the Henry Royce Institute (Grant No. ref EP/R010145/1). For the purpose of Open Access, the author has applied a CC BY public copyright license to any Author Accepted Manuscript (AAM) version arising from this submission.

AUTHOR DECLARATIONS

Conflict of Interest

The authors have no conflicts to disclose.

Author Contributions

Yuelin Xiong: Data curation (equal); Formal analysis (equal); Investigation (equal); Methodology (equal); Visualization (equal); Writing – original draft (equal). **Ruidong Zhou**: Investigation (supporting); Writing – original draft (supporting). **Anastasia Soeriyadi**: Data curation (supporting); Formal analysis (supporting); Investigation (supporting); Methodology (supporting); Writing – original draft (supporting). **Zongtao Liu**: Data curation (equal); Formal analysis (equal); Investigation (equal); Methodology (equal). **Soumyajit Maitra**: Data curation (supporting); Formal analysis (equal); Investigation (supporting); Methodology (equal). **Yifu Shi**: Data curation (supporting); Investigation (supporting). **Jingyan Chen**: Data curation (supporting); Investigation (supporting). **John O'Sullivan**: Investigation (supporting); Visualization (lead). **Matthew Wright**: Investigation (supporting); Writing – review & editing (equal). **Pietro Altermatt**: Methodology (supporting); Supervision (supporting). **Ruy Sebastian Bonilla**: Conceptualization (equal); Investigation (equal); Project administration (equal); Resources (equal); Supervision (equal); Writing – review & editing (equal).

DATA AVAILABILITY

All data created during this research and published in this article are openly available from the Oxford University Research Archive and can be downloaded free of charge from http://ora.ox.ac.uk.

REFERENCES

[1] Y. Zhang, M. Kim, L. Wang, P. Verlinden, and B. Hallam, "Design considerations for multi-terawatt scale manufacturing of existing and future photovoltaic technologies: Challenges and opportunities related to silver, indium and bismuth consumption," Energy Environ. Sci. **14**(11), 5587–5610 (2021).

[2] J. D. Fields *et al.*, "The formation mechanism for printed silver-contacts for silicon solar cells," Nat. Commun. **7**(1), 11143 (2016).

[3] N. Balaji, M. C. Raval, and S. Saravanan, "Review on metallization in crystalline silicon solar cells," in *Solar Cells* (IntechOpen, 2020).

[4]Verband Deutscher Maschinen- und Anlagenbau e.V. (VDMA), International Technology Roadmap for Photovoltaic (ITRPV), 2023.
[5]K. Tsuji, S. Suzuki, M. Dhamrin, A. Adrian, T. Buck, and N. Usami, "Fine line screen-printing aluminum for front side p^+ metallization of high efficiency solar cells," AIP Conf. Proc. **2487**, 130014 (2022).
[6]V. A. Popovich, M. Janssen, I. M. Richardson, T. van Amstel, and I. J. Bennett, "Microstructure and mechanical properties of aluminum back contact layers," Sol. Energy Mater. Sol. Cells **95**(1), 93–96 (2011).
[7]F. S. Grasso, L. Gautero, R. Preu, and R. Lanzafame,"Characterization of aluminium screen-printed local contacts," in *Proceedings of the 2nd Workshop on Metallization* (Konstanzer Online-Publikations-System, Konstanz, 2010), pp. 15–21.
[8]R. Lago *et al.*, "Screen printing metallization of boron emitters," Prog. Photovoltaics: Res. Appl. **18**(1), 20–27 (2010).
[9]N. Wöhrle, E. Lohmüller, J. Greulich, S. Werner, and S. Mack, "Towards understanding the characteristics of Ag–Al spiking on boron-doped silicon for solar cells," Sol. Energy Mater. Sol. Cells **146**, 72–79 (2016).
[10]A. K. Sharma, S. Mitra, S. Behera, and P. K. Basu, "Exploring the efficiency limiting parameters trade-off at rear surface in passivated emitter rear contact (PERC) silicon solar cells," Sol. Energy Mater. Sol. Cells **232**, 111338 (2021).
[11]J. Szlufcik *et al.*, "Laser ablation of SiO_2/SiN_x and AlO_x/SiN_x back side passivation stacks for advanced cell architectures," in *Proceedings of the 26th European Photovoltaic Solar Energy Conference* (EU PVSEC, 2011), pp. 2180–2183.
[12]F. Qian, H. Shen, G. Huang, B. Liu, and J. Hong, "Improvement of laser-induced damage on high-efficiency solar cells via top-hat beam ablation," Energies **17**(4), 858 (2024).
[13]T. Hassel, A. Beniyash, and G. Klimov, "Non-vacuum electron beam welding and cutting of cupper," IOP Conf. Ser.: Mater. Sci. Eng. **759**(1), 012003 (2020).
[14]G. Heinrich, M. Bähr, K. Stolberg, T. Wütherich, M. Leonhardt, and A. Lawerenz, "Investigation of ablation mechanisms for selective laser ablation of silicon nitride layers," Energy Procedia **8**, 592–597 (2011).
[15]V. V. Rana and Z. Zhang, "Selective removal of dielectric layers using picosecond UV pulses," Proc. SPIE **7193**, 719321 (2009).
[16]M. D. Abbott, J. E. Cotter, F. W. Chen, T. Trupke, R. A. Bardos, and K. C. Fisher, "Application of photoluminescence characterization to the development and manufacturing of high-efficiency silicon solar cells," J. Appl. Phys. **100**(11), 114514 (2006).
[17]T. Trupke, R. A. Bardos, M. C. Schubert, and W. Warta, "Photoluminescence imaging of silicon wafers," Appl. Phys. Lett. **89**(4), 044107 (2006).
[18]C. Mader, R. Bock, J. Müller, J. Schmidt, and R. Brendel, "Formation of locally aluminum-doped p-type silicon regions by in-line high-rate evaporation," Energy Procedia **8**, 521–526 (2011).
[19]S. Guo, G. Gregory, A. M. Gabor, W. V. Schoenfeld, and K. O. Davis, "Detailed investigation of TLM contact resistance measurements on crystalline silicon solar cells," Sol. Energy **151**, 163–172 (2017).
[20]F. Zeng, Y. Feng, Z. Liang, and H. Shen, "Specific contact resistance measurements on C-Si solar cells by novel TLM method," in *2012 38th IEEE Photovoltaic Specialists Conference* (IEEE, 2012), pp. 000509–000513.
[21]P. N. Vinod, "Specific contact resistance measurements of the screen-printed Ag thick film contacts in the silicon solar cells by three-point probe methodology and TLM method," J. Mater. Sci.: Mater. Electron. **22**(9), 1248–1257 (2011).
[22]Y. Chen *et al.*, "Mass production of industrial tunnel oxide passivated contacts (i-TOPCon) silicon solar cells with average efficiency over 23% and modules over 345 W," Prog. Photovoltaics: Res. Appl. **27**(10), 827–834 (2019).
[23]A. Dabirian *et al.*, "Metallization of Si heterojunction solar cells by nanosecond laser ablation and Ni–Cu plating," Sol. Energy Mater. Sol. Cells **159**, 243–250 (2017).
[24]B. A. Kamino *et al.*, "Low-temperature screen-printed metallization for the scale-up of two-terminal perovskite–silicon tandems," ACS Appl. Energy Mater. **2**(5), 3815–3821 (2019).
[25]A. Cuevas, P. A. Basore, G. Giroult-Matlakowski, and C. Dubois, "Surface recombination velocity of highly doped *n* -type silicon," J. Appl. Phys. **80**(6), 3370–3375 (1996).
[26]C. Paul Mader, "In-line high-rate evaporation of aluminum for the metallization of silicon solar cells," Doctoral thesis (Leibniz Universität Hannover, 2012).
[27]V. Arya, S. Schellinger, T. Fellmeth, B. Steinhauser, B. Gruebel, and A. Brand, "TOPCon solar cells: Laser ablation and contact formation strategies," in *2020 47th IEEE Photovoltaic Specialists Conference (PVSC)* (IEEE, 2020), pp. 0401–0404.
[28]C. Mader, J. Muller, S. Gatz, T. Dullweber, and R. Brendel, "Rear-side point-contacts by inline thermal evaporation of aluminum," in *2010 35th IEEE Photovoltaic Specialists Conference* (IEEE, 2010) 001446–001449.
[29]J. Wong and R. Sridharan, Griddler: The handy 2D solar cell calculator, PV International Edition, 2014, Vol. 25.